RSC Advances

ROYAL SOCIETY OF CHEMISTRY

www.rsc.org/advances

Removal of As(III) from water using modified jute fibres as a hybrid adsorbent

Linlin Hao[a], Tong Zheng[a], Jiping Jiang[a], Qi Hu[a], Xilan Li[b], Peng Wang[a]*

[a] State Key Laboratory of Urban Water Resource and Environment, School of Municipal and Environmental Engineering, Harbin Institute of Technology, Harbin 150090, P. R. China

[b] State Key Laboratory of Physical Chemistry of Solid Surfaces, College of Chemistry and Chemical Engineering, Xiamen University, Xiamen 361005, P. R. China

* Corresponding author. Tel.: +86 451 86283801; fax: +86 451 86283801

E-mail address: pwang73@vip.sina.com

ABSTRACT

Many studies concentrated on the arsenic removal from water using granular mineral fine particles. However, very little researches focused on the preparation of materials which aimed to be applied to the situations of arsenic pollution emergencies in rivers or lakes. In this study, Jute fibre was modified by loading iron oxyhydroxide (which was demonstrated to be mainly α-FeOOH) to produce an effective hybrid adsorbent (Fe-JF) with the advantages of an excellent arsenic removal effect and easy of retrieval from rivers or lakes. Jute fibre was firstly esterified with succinic anhydride to graft with carboxyl groups in order to enhance the loading amount of Iron(III), the maximum Iron(III) loading on Fe-JF reached 208.2±0.2mg/g while the density of grafted carboxyl groups was 2.78 mmol/g. The maximum adsorption capacity for As(III) reached 12.66 mg/g while the density of carboxyl was 2.21 mmol/L. Meanwhile, the iron leaching amount was 0.178 mg/L which could meet the requirement of standard limit of iron in drinking water (China, 0.3 mg/L). Influencial factors, such as pH, contact time and coexisting anions were investigated in this study. The column experiments showed that the breakthrough point declined from 2300 BV (bed volumes) to 1200 BV when EBCT (empty-bed contact time) decreased from 3.5 min to 1.8 min. The Adams-Bohart model was adopted to describe the continuous flow system.

Keywords: As(III) (arsenite); Jute fibres; Adsorption; α-FeOOH; Carboxyl groups

1. Introduction

In China, with the rapid development of economy and urbanization process, sudden water pollution accidents occur frequently in recent years. These malignant water pollutions have resulted in severe environmental problems. [1] Among these accidents, arsenic contamination has attracted much attention because it is most frequently occurred. For instance, the groundwater of Huaihua city of Hunan province suffered arsenic contamination in 2008；Dasha river of Henan province was severly polluted by the illegal arsenic emissions of chemical factory; Yangzonghai lake of Yunnan province suffered arsenic contamination because of the As-containing wastewater without effective treatment；One particularly serious event was arsenic contamination in the Picang river of Shandong province in 2009, malignant pollution emergencies relating to arsenic happened twice in a short span of three months.

Adsorption was considered as a promising method to apply to arsenic polluted water remediation among the conventional methods of chemical precipitation, flocculation, membrane separation, ion exchange and so on. The key of adsorption is the appropriate adsorbent, thus seeking an effective and economic adsorbent has been thought of by many researchers. Activated carbon is the most commonly used adsorbent throughout the world. However, it is still facing some problems related to high cost, non-selectivity and its complicated regeneration requirement. [2, 3]

Although many mineral adsorbents such as goethite, ferrihydrite, akaganéite and lepidocrocite have been reported as having high affinity toward arsenic, they cannot be applied in arsenic contamination emergencies because of their tiny size and not easy to retrieve from water. Therefore, many supporters including sands, activated carbon, ion exchange resin and waste natural material have been selected to be loaded with tiny sized active components. [4, 5] In recent years, there have been many studies

68 focused on the bio-composites-based materials, [6-8] which were considered to be a
69 promising direction in the preparation of adsorbents applied to heavy metals removal
70 from water. It was reported that a novel hybrid material was produced by combining
71 γ-Fe_2O_3 and biochar, which exhibited an excellent ferromagnetic property, the highest
72 adsorption capacity for arsenate reached 3.15 mg/g. [9] Hristovski, etc. [10] investigated
73 the effect of synthesis conditions on iron (hydr)oxide impregnated activated carbon,
74 the iron content of the hybrid adsorbent ranged from 0.5 to 16% Fe/g of dry media.

75 As an adsorbent, jute would be a promising material because it is a commonly
76 available economic crop which could be obtained by a large quatity. It was reported
77 that Shukla and Pai [11] used a modifed jute fibre to remove Cu(II), Ni(II) and Zn(II)
78 from aquous solutions and achieved satisfactory results. The jute fibre can be easily
79 manipulated and is applicable to various situations, especially for rapid environmental
80 remediation after arsenic pollution accidents. The exhausted adsorbents could be
81 burned, to produce little arsenic-containing ash, which can be further treated through
82 immobilization technology. In addition, fibrous adsorbent showed lower water
83 resistance than granular adsorbents and could be woven into various shapes. [12] This
84 indicated that the fibrous adsorbents have the most potential market prospect.

85 Many studies have demonstrated that iron, including zero-valent iron, iron
86 oxy-hydroxides and iron minerals, have high affinity toward arsenic. [13-15] In our study,
87 the raw jute was firstly grafted with carboxylic groups, and then was complexed with
88 ferric ions, NaOH solution was added dropwise to form iron oxyhydroxide, which
89 was the major reactive center responsible for arsenic removal. [16] The aim of
90 introducing carboxylic groups was to increase the Iron(III) amount complexed on the
91 jute fibres. This study focused on As(III) removal from water because As(III) is more
92 toxic and more frequently occurs in environmental emergencies than As(V).

2. Materials and methods

2.1 Preparation of Fe-JF

(1) **Preparation of carboxylated jute fibres.** A total of 10 g pretreated dry jute fibres was reacted with succinic anhydride under pyridine reflux (200 mL) at 90°C for 12 h in order to get the carboxylate-funtionalized jute fibres. The fibers were subsequently washed with acetone, anhydrous ethanol, and deionized water to remove the residual organic solvent on the fibers.

(2) **Impregnation of iron.** The introduction of Iron(III) was accomplished by immersing the carboxylate-funtionalized jute fibres into an aqueous solution of 0.05 M $Fe(NO_3)_3 \cdot 9H_2O$ solutions (pH was adjusted to be 7.0±0.2) for 12 h. After filtration the fibers were filled into a glass column of 25×500 mm, and then 0.5 mol/L NaOH was slowly dropped at a rate of 100±1 mL/h through the glass column for 2h. The fibers were then aged at room temperature for another 12h. The deionized water was constantly dropped into the column until the color of the effluent changed from yellow to be colorless. The product was finally dried at 50°C and stored for further use. The synthesis route is shown in Fig. 1.

2.2 Arsenic Adsorption equilibrium Tests

A stock solution of As(III) at a concentration of 1000 mg/L was prepared using sodium As(III) ($NaAsO_2$; AR). A series of 250 mL glasses of the solution were added to 100 mL of 1, 5, 10, 25, 50, 80, 100, 120, 150 mg/L arsenic solutions and 0.5 g Fe-JF respectively. The samples were shaken at 150 rpm at room temperature for 24 h with pH adjusted to 7.0±0.1 with dilute HNO_3 or NaOH solutions.

2.3 Arsenic adsorption kinetics

The kinetics experiments were conducted in a round glass reactor that was placed in a thermostat water bath, where the temperature could be adjusted to different

degrees. A pH electrode combined with a thermometer was inserted below the surface of the solution to maintain a constant pH condition in the reactor.

2.4 Effect of pH and competing anions on arsenic removal

The initial As(III) concentration was 10 mg/L. The pH level was adjusted in the range of 3-10. The samples were adjusted several times during the initial 6 h to maintain the stability of the desired pH. The co-existing anions were prepared including Cl^-, SO_4^{2-}, NO_3^-, F^-, PO_4^{3-}, SiO_3^{2-}, their respective concentration was listed in Table 1, the initial As(III) concentration was 0.05 mg/L.

2.5 Fixed bed column experiments

A glass column of 22×200 mm was employed with a bed depth of 50 mm. A nylon mesh (1000 μm opening size) was placed at the bottom of column to prevent Fe-JF from being discharged into the tubes. The feed solution was prepared from 0.5 mg/L arsenic. The aqueous solution was pumped through the packed column with a peristaltic pump (BT-200B, Shanghai Qingpu analytical instrument Co., China).

2.6 Analytical methods

The density of carboxyl groups on the jute fibres were determined by back-titration method. [17] An amount of 0.1 g carboxylated jute fibres was suspended in 100mL of 0.01mol/L NaOH solution for 1 h under constant stirring. After filtration, the excess of NaOH was back-titrated with 0.01mol/L HCl solution. Methyl orange was used as an indicator and the titration was terminated when the solution color turned from yellow to orange. The density of carboxyl group was calculated by:

$$C_{\mathrm{COOH}} = \frac{(C_{\mathrm{NaOH}} V_{\mathrm{NaOH}}) - (C_{\mathrm{HCl}} V_{\mathrm{HCl}})}{m_{\mathrm{jute}}} \quad (1)$$

The SEM images were obtained using Quanta 200 FEG (USA), which was coupled with EDS system. The samples were pretreated with gold spraying in order to

enhance the conductivity and make it easier to observe for non-conductive samples. Total dissolved As and Fe levels were determined using an inductively coupled plasma emission spectrometer (ICP-OES) (PerkinElmer, Optima 2000, UK). For the experiments with intial As(III) concentration below 0.05 mg/L, the arsenic analytical method was hydride generation - atomic fluorescence spectroscopy (HG-AFS) (AFS-930, Beijing Jitian Co., Ltd, China), which is capable of detecting arsenic as low as 1.0 μg/L. All the samples were reduced by 5% (w) thiourea – 5% (w) ascorbic acid to ensure that all arsenic species were converted to detectable As(III). Iron(III) loaded on Fe-JF was extracted by HNO_3 (98%,V/V).

3. Results and discussion

3.1 Characterization of Fe-JF

The synthesized adsorbent has a fibrous shape and an excellent mechanical strength. The highest content of Fe loaded on the fibers was 208±2 mg of Fe/g after three cycles of loading process.

The photos of the raw and modified jute fibres are shown in Fig. 2 (a, b). The BET surface areas of raw jute are only 0.57 m^2/g. As shown in Fig. 2 (c), the jute surface is smooth and it is composed of very few pores. The elemental composition of the raw jute (as shown in the square of Site 1 (S1) in Fig. 2 (c)) is listed in Table. 2. The modified jute fibres develop a deep brown color due to the disperson of iron oxyhydroxide. Fig. 2 (d) show that the modified jute surface presents to be heterogeneous, Site 2 (S2) and Site 3 (S3) are selected for EDS analysis (the conducting medium of Au is deducted). The main metallic element contained in the square area (as in Fig. 2 (d, f)) is iron, with the percentage content varying from 25.78~34.02 %. The EDS spectra of Fe has two peaks: the high energy (K line：6.3996 keV) and low energy (L line: 0.7048 keV).

The FTIR spectrums of raw jute fibres and Fe-JF are shown in Fig. 3, where the wide band is seen at 3400 cm^{-1} due to —OH stretching vibration, and the characteristic absorption peaks of the cellulose backbone appeared at 1034 cm^{-1} and 1059 cm^{-1}. The raw jute was pretreated with 5% (w/v) NaOH solution in order to remove the adherent impurities. Compared with raw jute fibres, the FTIR spectrum of carboxylated jute showed two typical bands at 1721cm^{-1} and 1194cm^{-1}, which are attributed to the stretching C=O vibration and stretching C-O of COOH, respectively. [18] This indicated that carboxyl groups were successfully grafted onto the jute fibres cellulose.

To examine the iron mineral phase loaded on jute fibres, the samples are detected by X-ray diffraction (XRD) as shown in Fig. 4, The peaks at 2θ=17.8°, 21.2°, 26.7°, 33.2°, 34.7°, 36.6°, 40°, 41.2°, 47.3°, 50.6°, 53.2° , 59° , 61.4° are assigned to α-FeOOH and 2θ=26.7°, 39.2°, 61.1° are assigned to β-FeOOH. [19] Fig. S1 gives the standard XRD patterns of the referenced four kinds of iron (oxy-hydr)oxide and the main characteristic reflections are summarized in Table. 3. It can be considered that the iron oxyhydroxide loaded on jute fibres are mainly α-FeOOH and β-FeOOH. It is seen that the crystallinity of the products is poor, resulting from various kinds of iron oxyhydroxide particles mixed together, which are too small to diffract.

3.2 Relationship of the density of carboxyl groups to Iron(III) amount loaded on Fe-JF

The density of carboxyl groups were determined by back-titration method, where samples with different densities of carboxyl groups were obtained by changing the esterification reaction time of 4, 8, 12 h during the synthesis procedure. As shown in Table 4, when the density of carboxyl groups increased from 1.19 to 2.78 mmol/g, the Fe content also increased from 124±2 to 208±2 mg of Fe/g. However, the iron shed to

the bulk solutions increased simultaneously from 0.06 to 0.52 mg of Fe/g. The raw jute fibre could also adsorb iron(Ⅲ) as high as 102±2 mg/g, but the iron leaching amount reached 10.12 mg/g, the excess leaching of iron into water may cause the secondary pollution. The results indicated that the carboxylated jute fibre could greatly reduce the iron leaching from the hybrid material.

In order to uncover the reason of Fe leaching, the iron oxyhydroxide loaded D113 (Styrene type - weak acid cation exchange resin) containing a high density of fixed —COOH groups (3.26 mmol/g) was prepared following identical procedures. The result showed that the Fe content loaded on the resin reached 290±3 mg of Fe/g, but the iron shed to the bulk solutions was only 0.012 mg/g, which was much lower than that of the jute fibres. Therefore we deduced that the comparatively higher leaching of iron was attributed to the swelling of cellulose due to the long time soaking in water.

3.3 Adsorption equilibriums

Adsorption equilibrium tests were carried out to investigate the adsorption capacities at various initial concentrations at pH 7.0±0.1. Figure 5 showed that the carboxylated jute surface enhanced the ability to uptake ferric ions, thus greatly increasing the content of loaded iron oxyhydroxide. The iron loading amount of the raw jute was 102±2 mg/g, which was significantly increased to 124±2 mg/g with the density of grafted carboxyl of 1.19 mmol/g. When the density of grafted carboxyl was enhanced from 1.19 to 2.78 mmol/g, the loading iron was accordingly increased to 208±2 mg of Fe/g. The adsorption capacity increased with an increase of carboxyl groups densities because the more carboxyl groups mean the more anchor locations available for combining with ferric ions, thus resulting in a higher amount of loaded iron oxyhydroxide.

The adsorption equilibrium data were fitted with Langmuir and Freundlich

isotherm models. The Langmuir isotherm equation was expressed as below: [20]

$$\frac{C_e}{q_e} = \frac{C_e}{q_{\max}} + \frac{1}{q_{\max} K_L} \quad (2)$$

Where q_e is the quantity of the species adsorbed at equilibrium (mg/g), K_L is a constant representing the virtual bonding strength between the target species and adsorbent, C_e is the equilibrium concentration of adsorbate in the solution, and $q_{\max}$ is the maximum adsorption capacity.

The Freundlich isotherm equation was expressed as follows: [21]

$$\ln q_e = \ln K_F + 1/n \ln C_e \quad (3)$$

where q_e is the quantity of the species adsorbed at equilibrium (mg/g), K_F is a constant which is a measure of sorption capacity, $1/n$ is a measure of adsorption density, and C_e is the equilibrium concentration of adsorbate in the solution.

The isotherms fitting parameters were listed in Table 5, the maximum adsorption capacity was 12.66 mg/g. Higher values of constant k_L and n indicated the easier uptake of As(III). The results appeared to be similar with arsenic adsorption behavior of iron oxyhydroxide fine powders. [16] Compared with iron oxide-coated sand (Q_{max}=0.04 mg/g), [22] Fe-JF showed much higher adsorption capacity, which was attributed to the high amount of loaded iron and the appropriate iron mineral phase of α-FeOOH. The comparison of the Langmuir capacity of more adsorbents for arsenic adsorption was listed in Table 6.

3.4 Adsorption kinetics

The time dependence of As(III) adsorption process is shown in Fig. 6. The initial uptake rate was rapid, and then was followed by a slower reaction rate that gradually approached equilibrium. About 70% As(III) was removed during the first 60 mins. The slower adsorption occurred due to the decrease in the driving concentration difference between bulk solution and Fe-JF surface. The adsorption achieved

equilibrium within 200 min when 80% As(III) was removed.

Several kinetic models such as pseudo-first-order, pseudo-second-order, Elovich equation, were used to investigate the adsorption mechanism. [39]

The pseudo-first-order kinetic equation is expressed as follows: [39]

$$\log(q_e - q_t) = (\log q_e) - k_1 t \quad (4)$$

Where t is the time, q_t is adsorption capacity at t, k_1 (min^{-1}) is the rate constant.

The pseudo-second-order equation could be expressed as: [40]

$$\frac{t}{q_t} = \frac{1}{k_2 q_e^2} + \frac{1}{q_e} t \quad (5)$$

where t is the time, q_t is adsorption capacity at t, q_e is the adsorption equilibrium capacity, k_2 ($g \cdot mg^{-1} \cdot min^{-1}$) is a constant which strongly depended on the applied operating conditions such as the initial solute concentration, pH, temperature and so on.

The Intraparticle diffusion equation is expressed as follows: [40]

$$q_t = k_d t^{1/2} + C \quad (6)$$

where t is the time, q_t is adsorption capacity at t, k_d ($mg \cdot L^{-1} \cdot min^{-1/2}$) is the rate constant. A plot of q_t versus ln(t) should yield a straight line if kinetic curves follow Elovich equation.

Among the three kinetic models, the pseudo-second-order described the experimental data best, where the determinant coefficients (R^2) were all above 0.99. The arsenic removal process is presumed to involve three stages: (1) mass transfer across the external boundary layer; (2) diffusion within the pores of the adsorbent; (3) adsorption at a special site on the surface. Good conformation to Intraparticle diffusion equation suggests that the rate-determing step is the diffusion within the pores of adsorbents, many literatures reported that porous materials or iron loaded

porous materials usually fit well to Intraparticle diffusion equation. [41] In this study, diffusion is not likely to be rate-limiting due to the smooth surface of jute fibres and the agitation condition. Results showed a good fit to the pseudo-second-order model with the correlation coefficient above 0.999, indicating that As(III) adsorption onto Fe-JF was dominated by the chemical process.

3.5 Effect of pH

The uptake of As(III) as a function of pH ranging from 3 to 10 is shown in Fig. 7. The percentage removal did not change much in the range of pH 3-8, but was obviously reduced from ca. 85% to ca. 55% when pH shifted from 8 to 10. The optimal adsorption condition was found between pH 3-8, which is in accordance with the pH of natural water and there is no necessary to pre-adjust the pH for As(III) contaminated natural water body when Fe-JF is applied to As(III) remediation.

The aqueous pH is one of the most important factors that influence the adsorption efficiency. As(III) appears to be different species in the wide pH range of 3-10. From Eqs. (7) to (9), As(III) exists mostly as neutral H_3AsO_3 when the pH is lower than 9, while mono-valent $H_2AsO_3^-$ is the stable form at pH between 9-12. [3, 42]

$$H_3AsO_3 \leftrightarrow H_2AsO_3^- + H^+ \qquad pK_{a1}=9.2 \tag{7}$$

$$H_2AsO_4^- \leftrightarrow HAsO_4^{2-} + H^+ \qquad pK_{a2}=12.1 \tag{8}$$

$$HAsO_4^{2-} \leftrightarrow AsO_4^{3-} + H^+ \qquad pK_{a3}=12.7 \tag{9}$$

Cumbal and SenGupta [43] reported the distribution of three surface functional groups of iron oxyhydroxide (e.g., $FeOOH_2^+$ (pH<6.5), FeOOH (6.5<pH<9), and $FeOO^-$ (pH>9)) changed with respect to pH. Electrostatic repulsion is not dominated since neutral H_3AsO_3 is stable at pH 3-8, which was consistent with the slight change of percentage removal at pH 3-8. The adsorption of As(III) onto iron oxyhydroxide of Fe-JF surface is mainly by ligand exchange (Eqs.(10), (11)) while electrostatic

attraction is insignificant. The remarkable decline between pH 8-10 was attributed to the electrostatic repulsion between $FeOO^-$ and $H_2AsO_3^-$ (Eqs.(12), (13)).

$$FeOOH_2^+ + H_3AsO_3 \leftrightarrow FeOH_2AsO_3 + H_2O + H^+ \quad (10)$$

$$FeOOH + H_3AsO_3 \leftrightarrow FeOH_2AsO_3 + H_2O \quad (11)$$

$$FeOO^- + H_2AsO_3^- \leftrightarrow FeOHAsO_3^- + OH^- \quad (12)$$

$$FeOO^- + HAsO_3^{2-} \leftrightarrow FeOAsO_3^{2-} + OH^- \quad (13)$$

3.6 Effect of co-existing anions

In natural water sources such as rivers and lakes, many anions might exist together. The effects of those co-existing anions, including Cl^-, SO_4^{2-}, NO_3^-, F^-, SiO_3^{2-}, on As(III) adsorption by Fe-JF have been studied, their effects were shown in Fig. 8. When the dosage of Fe-JF was 2 g/L, the residual arsenic concentration decreased from 0.008 mg/L to 0.006 mg/L in the presence of these co-existing anions, the results showed that the presence of Cl^-, SO_4^{2-}, NO_3^-, F^-, SiO_3^{2-} have a slightly adverse effect for As(Ⅲ) removal. Among all the co-existing anions, sulfate is considered to be in greater competition due to the enhanced electrostatic interaction, but it was still uncertain to determine whether an outer or inner sphere complex forms. Phosphate was often reported to have a profound competing impact on arsenic adsorption onto iron hydroxide, it is not difficult to understand that Phosphorus and Arsenic are in the same main group, PO_4^{3-} and AsO_4^{3-} have an identical chemical structure, and both molecules are tetrahedral oxyanions with similar pK_a values. Experiments were conducted with 0.1 mg/L phosphates in order to investigate the effect of competition from phosphates. As can be seen from Fig. 8, phosphates caused an essential drop in As(Ⅲ) removal efficiency, the maximum removal efficiency decreased from 98% to 90%. The interference effects of phosphates are may attributed to the competition for

active sites.

3.7 Fixed-bed column runs

The column adsorption experiments were conducted at a neutral pH level. As shown in Fig. 9, at an EBCT of 3.5 min and the SLV (superficial liquid velocity) was 0.86 m/h, the effluent concentration of As(III) was well below the breakthrough point of 0.01 mg/L with the bed volumes less than 2300 BV (bed volumes), and then the effluent As(III) concentration began to increase significantly. When the effluent concentration reached 90% of the initial concentration, the adsorption column was considered to be exhausted. EBCT is an important parameter and the bigger EBCT results in a slower feed flow rate. Generally, the bed volumes of breakthrough point are increased with a decrease in EBCT, this is also proved in our study. When the EBCT decreased from 3.5 min to 1.8 min, the breakthrough point declined from 2300 BV to 1200 BV. The large decrease of ca. 50% indicates that the uptake efficiency depend strongly on contact time. These results accord with the kinetics results that Fe-JF needs a comparatively longer time to reach equilibrium, many literatures reported that a lower kinetic performance was more sensitive to EBCT [44].

The detailed numerical results are given in Table 7, breakthrough capacities (until breakthrough point of 0.01 mg/L was observed) for As(III) were 9.63 and 5.02 mg/g respectively at EBCT of 3.5 and 1.8 min, values which are much lower than the saturated adsorption capacity of 12.66 mg/g because the terminal mass transfer unit was not fully adsorbed. Moreover, the compacting effect in the column and channel flow may lead to the insufficient contact between Fe-JF and water. Breakthrough capacity decreased significantly from 9.63 to 5.02 mg/L indicated the flow rate had a significant influence on the removal efficiency. The higher flow rate lowered the full contact time between Fe-JF and As(III) species, thus resulting in an increase of

effluent arsenic concentration.

Several models were widely used to simulate the column tests data, i.e. thomas, Yoon-Nelson, Wolborska and Adams–Bohart models. The adams-bohart model is used in this study to describe the initial part of the breakthrough part, the model was described as the following equation: [45]

$$\ln \frac{C_t}{C_0} = K_a C_0 t - \frac{K_a N_0 x}{U_0} \quad (14)$$

where, the parameters N_0 means the saturation concentratin of the column bed (mg/L), K_a is the adsorption rate constant (L/mg • h), x is the column bed depth (m), U_0 represents the empty bed flow linear velocity (m/h).

The parameters of N_0 and K_a can be determined from a linear plot of ln (C_t/C_0) versus time at given flow rate and bed depth. A linear relationship between ln (C_t/C_o) versus t is obtained for the initial part (before breakthrough point) is shown in Fig. S2. Respective values of N_0 and K_a are presented in Table. 7.

Conclusion

The present work indicates that the modified jute fibres (Fe-FJ) possess more efficiency in adsorbing As(III) than the raw jute fibres. The loading amount of Fe is increased with an increase in grafted carboxyl group densities. XRD patterns indicate that the loaded iron oxyhydroxide was mainly α-FeOOH. The adsorption is governed by Langmuir model giving extremely good fit. The optimal adsorption performance is achieved at around neutral pH, there is no obviously adverse effect of common co-existing anions for As(III) adsorption. Flow rate has a significant influence on the removal rate. The saturation concentration simulated by Adamas-Bohart model is found to be 159.21 mg/L at the EBCT of 3.5 min. From a practical viewpoint, this novel fibrous material has advantages for practical application because of its quite

effective cost and ease of retrieval from water.

Acknowledgments

This work was supported by the Funds for Creative Research Groups of China (Grant No. 51121062) National Water Pollution Control and Management Technology Major Projects (2012ZX07205-005).

References

1 Q. Hu, D.-W. Gao, H.-Y. Pan, L.-L. Hao, P. Wang, *RSC Adv.*, 2014, **4**, 40071-40077.

2 A. Demirbas, *J. Hazard. Mater.*, 2009, **167**, 1-9.

3 D. Mohan, C.U. Pittman Jr, *J. Hazard. Mater.*, 2006, **137**, 762-811.

4 S.N. Kartal, Y. Imamura, *Bioresour. Technol.*, 2005, **96**, 389-392.

5 H. Xu, B. Allard, A. Grimvall, *Water Air Soil Pollut.,* 1991, **57**, 269-278.

6 A. Özer, *J. Hazard. Mater.*, 2007, **141**, 753-761.

7 A. Özer, H. Pirincci, *J. Hazard. Mater.*, 2006, **137**, 849-855.

8 W. Wan Ngah, M. Hanafiah, *Bioresour.Technol.,* 2008, **99**, 3935-3948.

9 M. Zhang, B. Gao, S. Varnoosfaderani, A. Hebard, Y. Yao, M. Inyang, *Bioresour. Technol.,* 2013, **130**, 457–462.

10 K. D. Hristovski, P. K. Westerhoff, T. Möllerc, P. Sylvester, *Chem. Eng. J.,* 2009, **146**, 237-243.

11 S. Shukla, R.S. Pai, *Bioresour. Technol.,* 2005, **96**, 1430-1438.

12 M.R. Awual, A. Jyo, T. Ihara, N. Seko, M. Tamada, K.T. Lim, *Water Res.,* 2011b, **45**, 4592-4600.

13 J.M. Calo, L. Madhavan, J. Kirchner, E.J. Bain, *Chem. Eng. J.,* 2012, **189**, 237-243.

14 S. Lin, D. Lu, Z. Liu, *Chem. Eng. J.,* 2012, **211**, 46-52.

15 Y. Glocheux, M. M. Pasarín, A.B. Albadarin, S.J. Allen, G.M. Walker, *Chem. Eng. J.,* 2013, **228**, 565-574.

16 M. Faria, R.S. Rosemberg, C.A. Bomfeti, D.S. Monteiro, F. Barbosa, L.C. Oliveira, M. Rodriguez, M.C. Pereira, J.L. Rodrigues, *Chem. Eng. J.,* 2014, **237**, 47-54.

17 H.P. Boehm, E. Diehl, W. Heck, R. Sappok, *Angew Chem. Int. Ed. Engl.,* 1964, **3**, 669-677.

18 A. Keranen, T. Leiviska, B.-Y. Gao, O. Hormi, J. Tanskanen, *Chem. Eng. Sci.,* 2013, **98**, 59-68.

19 X. Wang, X. Chen, L. Gao, H. Zheng, M. Ji, C. Tang, T. Shen, Z. Zhang, *J. Mater. Chem.,* 2004, **14**, 905-907.

20 V. Vinodhini, N. Das, *American-Eurasian Journal of Scientific Research*, 2009, **4**, 324-329.

21 Z. Akmar Zakaria, M. Suratman, N. Mohammed, W. Azlina Ahmad, *Desalination*, 2009, **244**, 109-121.

22 O. Thirunavukkarasu, T. Viraraghavan, K. Subramanian, *Water Air Soil Pollut.,* 2003, **142**, 95-111.

23 C. Daikopoulos, Y. Georgiou, A.B. Bourlinos, M. Baikousi, *Chem. Eng. J.,* 2014, **256**, 347–355.

24 Y. Tian, M. Wu, X.-B. Lin, P. Huang, *J. Hazard. Mater.,* 2011, **193**, 10–16.

25 T.-F. Lin, J.-K. Wu, *Water Res.,* 2001, **35**, 2049−2057.

26 J. Hlavay, K. Polyak, *J. Colloid Interface Sci.,* 2005, **284**, 71-77.

27 A. Maiti, S. DasGupta, J.K. Basu, S. De, *Sep. Purif. Technol.,* 2007, **55**, 350-359.

28 S.R. Kanel, B. Manning, L. Charlet, H. Choi, *Environ. Sci. Technol.,* 2005, **39**, 1291-1298.

29 V. Chandra, J. Park, Y. Chun, J.-W. Lee, *ACS Nano*, 2010, **4**, 3979–3986.

30 K. Gupta, A. Maity, U.C. Ghosh, *J. Hazard. Mater.,* 2010, **184**, 832-842.

31 J. Fang, Z.M. Gu, D.C. Gang, *Environ. Sci. Technol.*, 2007, **41**, 4748-4753.

32 D. Ociński, I. Jacukowici-Sobala, J. Raczyk, E. Kociolek-Balawejder, *React. Funct. Polym.,* 2014, **83**, 24-32.

33 D.N. Thanh, M. Singh, P. Ulbrich, N. Strnadova, *Sep. Purif. Technol.,* 2011, **82**, 93-101.

34 M. Zhang, B. Gao, S. Varnoosfaderani, A. Hebard, *Bioresour. Technol.,* 2013, **130**, 457-462.

35 K. Zhao, H.M. Guo, X.Q. Zhou, *Appl. Geochem.*, 2014, **48**, 184-192.

36 S. Kundu, A.K. Gupta, *J. Hazard. Mater.,* 2007, **142**, 97-104.

37 G.S. Murugesan, M. Sathishkumar, K. Swaminathan, *Bioresour. Technol.,* 2006, **97**, 483-487.

38 M. Mosaferi, S. Nemati, A. Khataee, S. Nasseri, *J. Environ. Health Sci. Eng.,* 2014, **12**, 69-74.

39 F.-C. Wu, R.-L. Tseng, R.-S. Juang, *Water Res.*, 2001a, **35**, 613-618.

40 X. Xu, B.-Y. Gao, Q.-Y. Yue, Q.-Q. Zhong, X. Zhan, *Carbohydr. Polym.*, 2010, **82**, 1212-1218.

41 W. Chen, R. Parette, J. Zou, F.S. Cannon, B.A. Dempsey, *Water Res.,* 2007, **41**, 1851-1858.

42 K. Wu, R. Liu, T. Li, H. Liu, J. Peng, J. Qu, *Chem. Eng. J.*, 2013, **226**, 393-401.

43 L. Cumbal, A.K. SenGupta, *Environ. Sci. Technol.*, 2005, **39**, 6508-6515.

44 M.R. Awual, A. Jyo, S.A. El-Safty, M. Tamada, N. Seko, *J. Hazard. Mater.*, 2011, **188**, 164-171.

45 B. Preetha, T. Viruthagiri, *Sep. Puri. Tech.,* 2007, **57**, 126-133.

439

440

441

442 Table 1

443 The list of the coexisting anions

Co-existing anions	Conc./mg/L
SO_4^{2-}	50
NO_3^-	2
SiO_3^{2-}	20
Cl^-	35
F^-	10

444

445

446

447 Table 2

448 Elemental analysis of raw sawdust and MSD (% based on dry weight)

Element	Content (*Wt* %)		
	Raw jute	Fe-JF	
	S1	S2	S3
C	54.62	45.20	42.90
O	42.71	29.02	23.08
Fe	--	25.78	34.02

449 -- means Not Detected.

450

451

452

453

454

455

456

457

458

459

460

461

462 Table 3

463 The XRD diffraction angles and corresponding crystal planes of five kinds of iron

464 (oxy-hydr)oxide.

Iron (oxy-hydr)oxides	Position [$^{o}2\theta$] Crystal plane									Reference
α-FeOOH	21.2 (100)	26.3 (120)	33.2 (130)	34.7 (021)	36.6 (111)	40 (121)	41.2 (140)	53.2 (221)	59.0 (151)	JCPDS 29-0713
β-FeOOH	11.8 (110)	16.8 (200)	26.7 (310)	35.2 (211)	39.2 (301)	46.4 (411)	52.0 (600)	55.9 (521)		JCPDS 34-1266
γ-FeOOH	14.1 (020)	27.1 (120)	36.3 (310)	38.1 (111)	46.9 (051)/ (200)	52.8 (151)				JCPDS 8-98
δ-FeOOH	35.2 (100)	39.9 (101)	54.4 (102)	63.2 (110)						JCPDS 13-87
α-Fe_2O_3	24.1 (012)	33.1 (104)	35.8 (110)	40.9 (113)	49.5 (024)	54 (116)	62.4 (214)	63.9 (300)	72 (1010)	JCPDS 33-0664

465

466

467

468

469

470

471

472

473

474

475

476

477

478

479

480 Table 4

481 The Iron(III) loading amount and leakage associated with different carboxyl groups

482 densities.

483

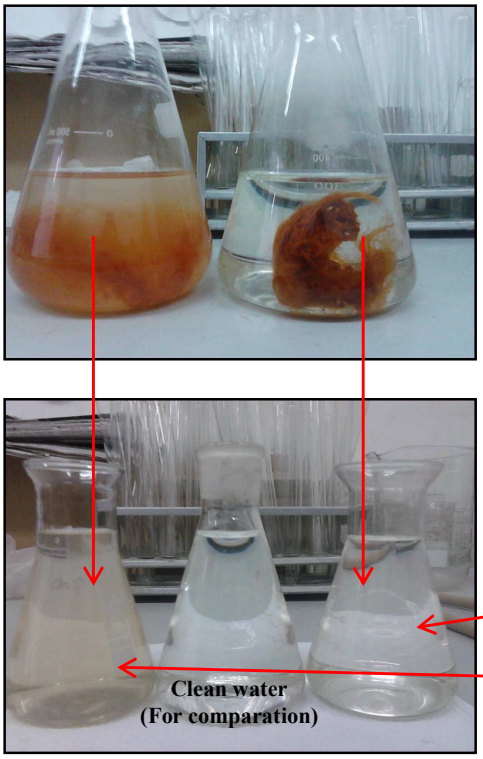

Table 4
The Iron(III) loading amount and leakage associated with different carboxyl groups densities.

Materials	Carboxylic (mmol/g)	Fe loading (mg/g)	Fe leaching (mg/g)
Fe-JF	1.19	124±2	0.061
	2.21	181±2	0.178
	2.78	208±2	0.518
Raw jute	0	102±2	10.12
D113	3.26	190±3	0.012

484

485

486

487

488

489

490

491

Table 5

Langmuir and *Freundlich* adsorption isotherms parameters of As(III).

As species	*Langmuir*			*Freundlich*			Fe content (mg/g)	max As/Fe (mol/mol)
	k_L	Q_{max}(mg/g)	R^2	K_f	n	R^2		
As(III)	0.167	11.49	0.984	1.721	2.203	0.985	124±2	0.069
	0.171	12.66	0.958	1.950	2.132	0.989	181±2	0.052
	0.210	13.69	0.980	2.499	2.409	0.974	208±2	0.049

Table 6. Comparison of the Langmuir capacity of different adsorbents for arsenic adsorption.

Adsorbents	Capacity (mg/g)		Reference
	As(III)	As(V)	
ZVI nanoparticles	3.5	--	[23]
Fe2O3 nanomaterial	1.25	--	[24]
Activated alumina	3.45	9.9	[25]
Iron hydroxide-coated alumina	7.65	15.9	[26]
Fe3O4 coated wheat straw	3.9	8.1	[24]
Natural laterite	0.17	--	[27]
Iron oxide-coated sand	0.029	0.14	[22]
Iron chitosan composite flake	16.15	--	[28]
Magnetite-reduced graphene oxide	10.20	5.27	[29]
Iron oxide@carbon	29.4		[30]
Iron modified activated carbon	--	6.57	[31]
Iron modified polymer	15.45	7	[32]
Perlite/γ-Fe2O3 composite	--	4.64	[33]
Biochar/ γ-Fe2O3 composite	--	3.147	[34]
Modified siderite	9.429	--	[35]
Iron oxide coated cement (~0.212 mm)	0.69	--	[36]
$FeCl_3$ treated tea fungal biomass	5.4	10.26	[37]
ZVI nanoparticles modified starch	12.2	14	[38]
Iron modified jute fibres	12.66	--	This work

Table 7

Column tests of As(III) uptake under two different EBCT.

EBCT (min)	Feed solution C_0 of As(III) (mg/L)	Bed depth (cm)	SLV (m/h)	Breakthrough point (BV)	Breakthrough capacity (mg/g)	Adams-Bohart model K_a (L/mg • h)	Adams-Bohart model N_0 (mg/L)
3.5	0.5	5	0.86	2300	9.63	0.69	100.05
1.8	0.5	5	1.67	1200	5.02	1.82	159.21

553

Figure captions

Fig. 1. Synthesis route used to obtain Fe-FJ.

Fig. 2. (a) Photo of the raw jute fibres. (b) Photo of the modified jute fibres. (c) SEM image of raw jute fibres (magnitude×5000). (d) SEM image of the modified jute fibres (magnitude×5000). (e) The EDS spectra of the modified jute fibres. (f) SEM image of the modified jute fibres (magnitude×10000).

Fig. 3. (A) FT-IR spectra of Raw jute fibres and Carboxylated jute fibres.

Fig. 4. X-ray diffraction pattern of iron oxyhydroxide loaded jute fibres.

Fig. 5. Adsorption isotherms for As(III) at different densities of carboxyl groups. (Fe-JF dosage 0.5 g, pH 7.0±0.2, temperature 25°C.)

Fig. 6. Kinetic adsorption data and pseudo-second order model fitting. (Initial As(III) concentration: 10 mg/L, Fe-JF dosage 1g, Fe content of Fe-JF 175±2 mg of Fe/g, pH 7.0±0.2, temperature 25°C.)

Fig. 7. Effect of pH on As(III) adsorption on Fe-JF. (Intial As(III) concentration: 10 mg/L, Fe-JF dosage 0.5 g, Fe content of Fe-JF 183±2 mg of Fe/g, temperature 25°C.)

Fig. 8. Effect of competing anions on As(III) adsorption on Fe-JF. (Intial As(III) concentration: 0.05 mg/L, Fe content of Fe-JF 172±2 mg of Fe/g, pH 7.0±0.2, temperature 25°C.)

Fig. 9. The schematic diagram of the dynamic column tests and As(III) breakthrough curves at different EBCT. (Initial As(III) concentration 0.5 mg/L, pH 7.0±0.2, Fe content of Fe-JF 181±2 mg of Fe/g, temperature 25±2°C)

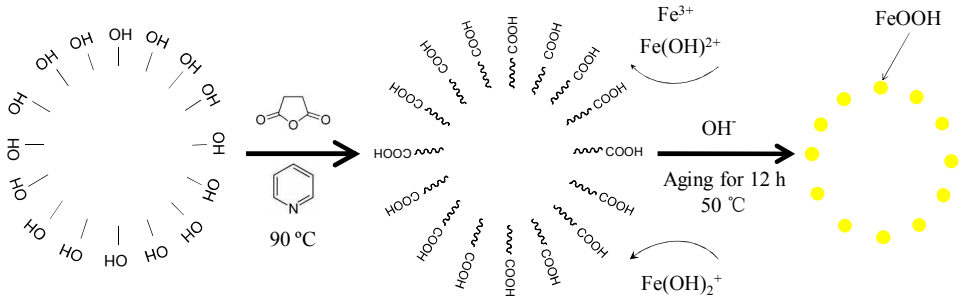

Fig. 1

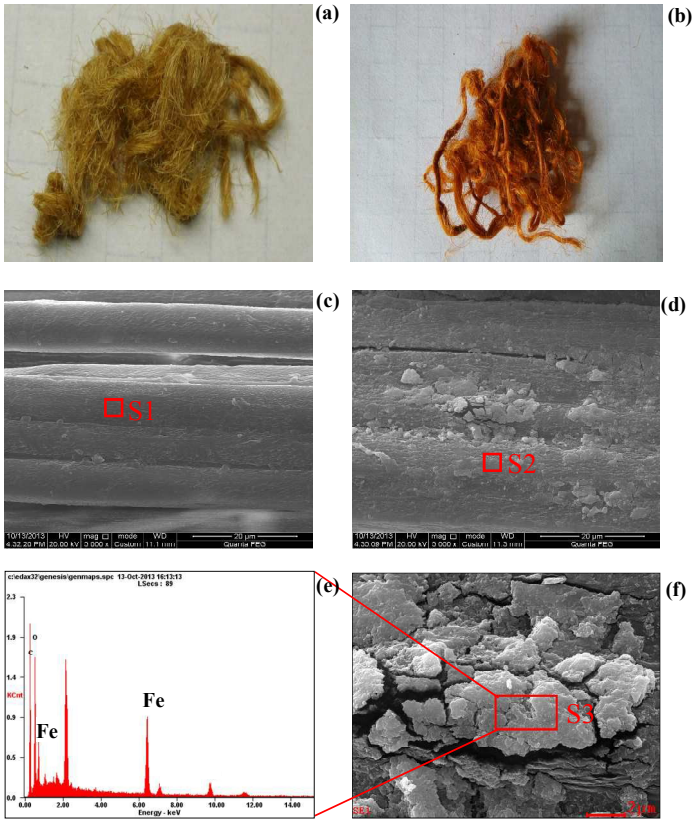

Fig. 2

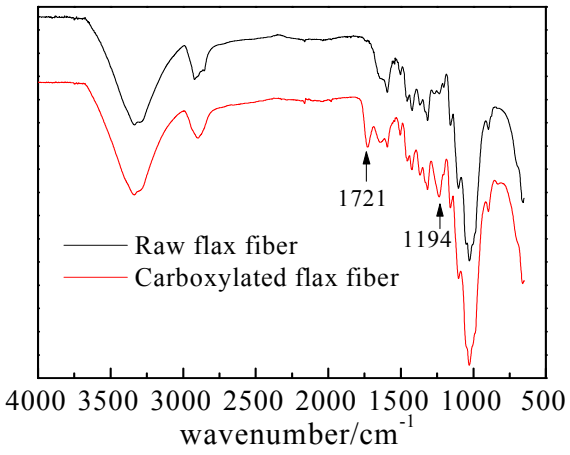

Fig. 3

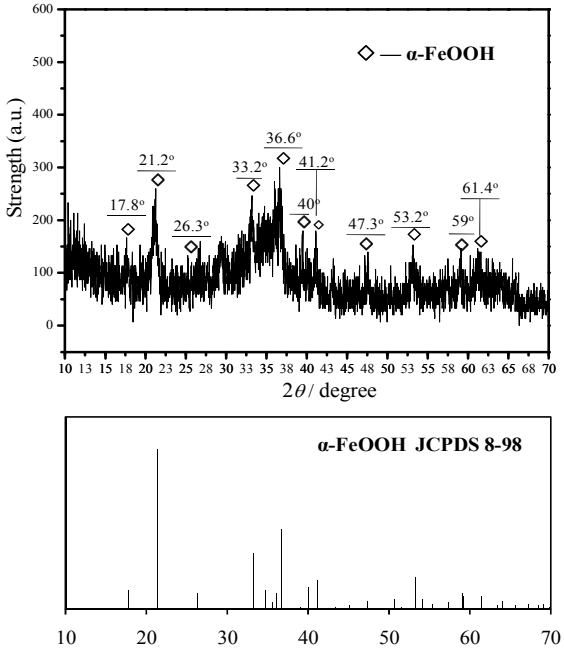

Fig. 4

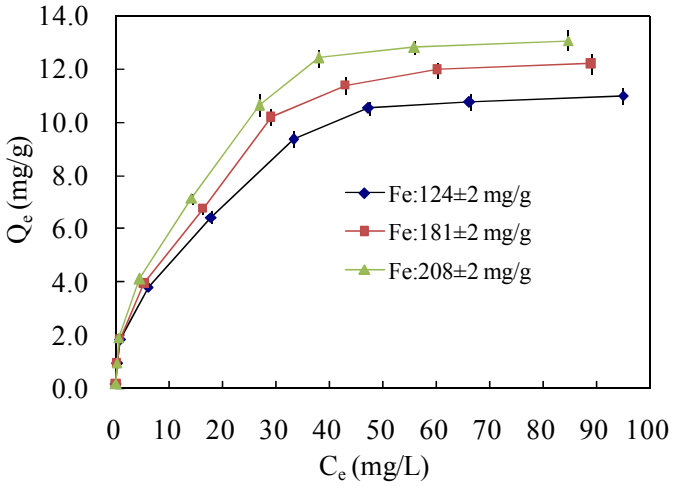

Fig. 5

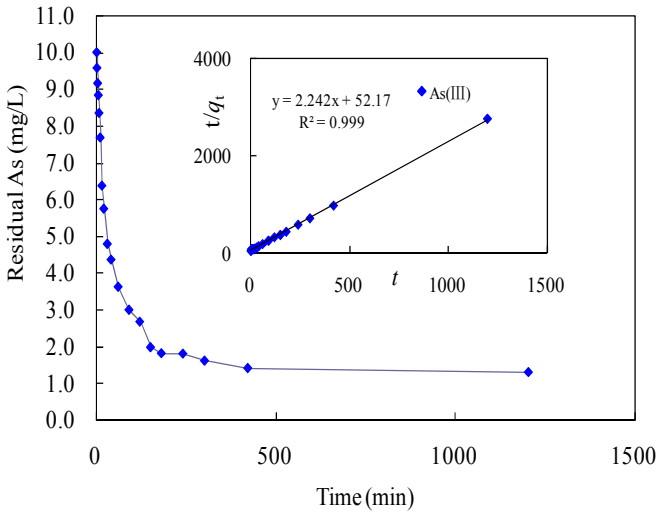

Fig. 6

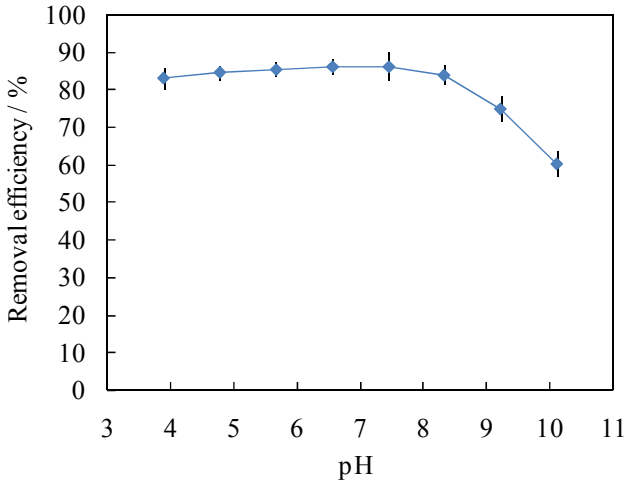

Fig. 7

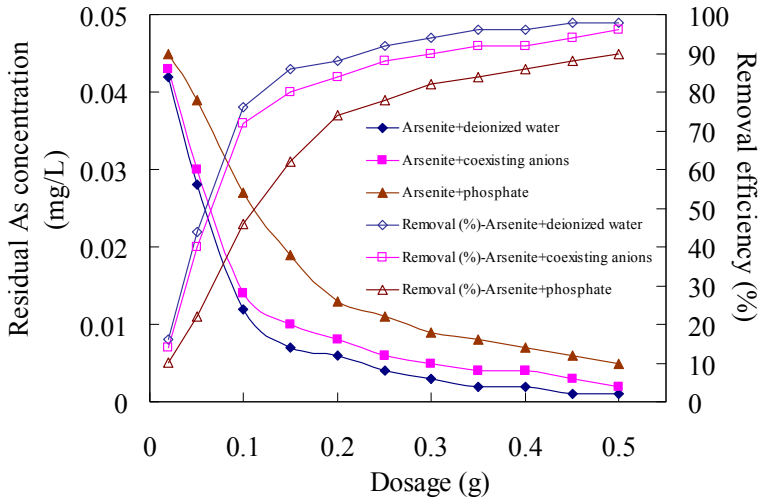

Fig. 8

187

188

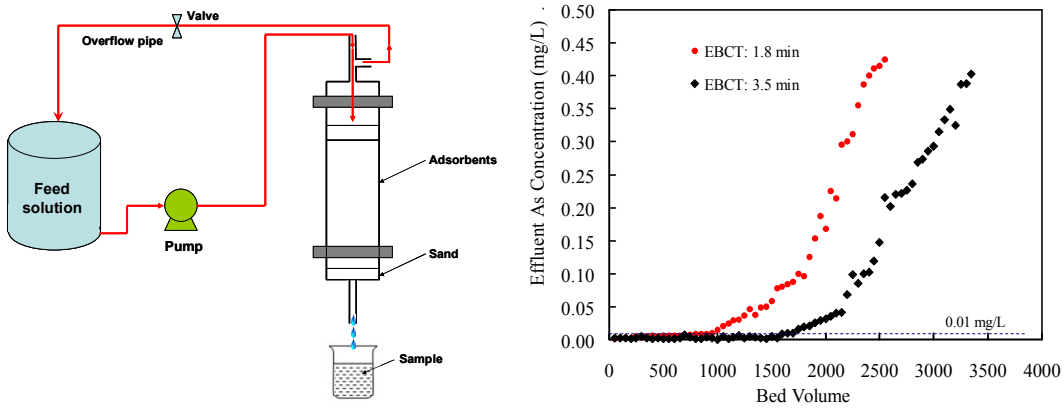

189

190 Fig. 9

191

192

193